ACS Catalysis

pubs.acs.org/acscatalysis Research Article

Enhancement of Alkyne Semi-Hydrogenation Selectivity by Electronic Modification of Platinum

Zhenshu Wang, Aaron Garg, Linxi Wang, Haoran He, Anish Dasgupta, Daniela Zanchet, Michael J. Janik, Robert M. Rioux,* and Yuriy Román-Leshkov*

Cite This: ACS Catal. 2020, 10, 6763−6770 Read Online

ACCESS | Metrics & More | Article Recommendations | Supporting Information

ABSTRACT: We demonstrate that atomically thin Pt shells deposited on transition metal carbide or nitride cores induce up to a 4-fold enhancement in C_2H_4 selectivity during the partial hydrogenation of acetylene compared with commercial carbon-supported Pt (Pt_{comm}) nanoparticles. While Pt typically catalyzes the complete hydrogenation of alkynes to alkanes, a catalyst comprising a nominal one monolayer (ML) Pt shell on titanium tungsten nitride cores (Pt/TiWN) is capable of net C_2H_4 generation under industrial front-end reaction conditions featuring a large excess of C_2H_4 and H_2. Microcalorimetry measurements are consistent with a change in the Pt electronic structure that decreases C_2H_4 binding strength, thus increasing partial hydrogenation selectivity. Density functional theory (DFT) calculations and X-ray absorption near edge structure (XANES) both indicate broadening of the Pt d-band and concomitant down-shifting of the d-band center. The ability to control shell coverage and core composition opens up extensive opportunities to modulate the electronic and catalytic properties of noble metal-based catalysts.

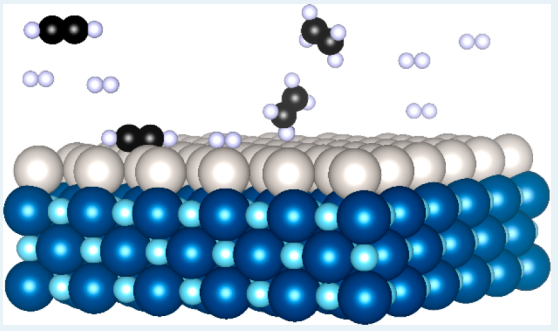

KEYWORDS: *core−shell nanoparticles, carbides, nitrides, electronic structure, acetylene semihydrogenation*

INTRODUCTION

Modulation of the electronic structure of supported metal nanoparticles enables an effective strategy for improving catalyst activity and selectivity.[1] This can be achieved by synthetic means to influence factors such as strong metal−support interactions,[2] number and type of under-coordinated sites (e.g., by synthesizing single atoms, nanoclusters, or particles with shapes that expose specific facets),[3−10] and synergies within heterometallic architectures, including alloys, intermetallics, and core−shells.[1,11−14] Core−shell structures offer a high degree of design flexibility given that the nanoparticle can be tuned by changing the size, shape, heterometallic core and shell composition, and extent of shell coverage.[15] Unfortunately, most core−shell nanoparticles suffer from dynamic alloying and restructuring during operation given the high miscibility of the elements in the structure.[16−19]

Recently, we reported that these challenges can be overcome by using transition metal carbides (TMCs) and nitrides (TMNs) as ideal core materials to host atomically thin late transition metal shells.[20−22] Specifically, our prior work reported the synthesis and characterization of such materials through a high-temperature exsolution methodology, where it was demonstrated that Pt shells bonded strongly with and wetted the surface of the metal-terminated TMC and TMN cores. Additionally, dynamic restructuring was eliminated because Pt is insoluble in the carbide and nitride lattices. These Pt/TMC and Pt/TMN core−shell nanoparticles featured enhanced CO tolerance during electro-oxidation reactions, an effect we hypothesized resulted from strong electronic interactions between the shell and the underlying ceramic core that altered the binding energy of the surface Pt-CO adsorbates.[20,21] While we envisaged this effect could influence other reactions over Pt catalysts for which the surface coverage of reactant-specific adsorbates in competitive reactions dictates selectivity, a fundamental study demonstrating this effect had not been performed.

Here, through a combination of rigorous reactivity studies, microcalorimetry, density functional theory (DFT) calculations, and X-ray absorption spectroscopy (XAS) measurements, we demonstrate the electronic structure (and thus catalytic performance) of Pt can be effectively tuned by depositing atomically thin shells onto titanium tungsten carbide or nitride cores. Specifically, we demonstrate the chemoselectivity of Pt for the partial hydrogenation of alkynes can be drastically enhanced using a core−shell architecture. Indeed, during polyethylene production, trace acetylene

Received: September 22, 2019
Revised: April 22, 2020
Published: May 12, 2020

https://dx.doi.org/10.1021/acscatal.9b04070
ACS Catal. 2020, 10, 6763−6770

(C_2H_2) impurities (~1.5%) in the ethylene (C_2H_4) feed need to be removed in order to avoid poisoning of the downstream polymerization catalysts. This requires a chemoselective catalyst capable of hydrogenating alkynes without saturating olefinic components. The binding energies of C_2H_2 and C_2H_4 on the catalyst surface play an important role in determining the C_2H_2 hydrogenation selectivity.[23,24] Several studies have shown Ag and Ga promoters in bimetallic Pd−Ag or Pd−Ga nanoparticles alter Pd through geometric and electronic effects to attain the desired binding energies of intermediates that maximize C_2H_4 selectivity.[25−27] While Pt is a remarkable hydrogenation catalyst, it is unselective for this reaction because it binds both C_2H_2 and C_2H_4 strongly, resulting in over hydrogenation to ethane (C_2H_6) at high C_2H_2 conversion.[27−29] In this study, we show that, unlike the combined geometric and electronic effects that change the catalytic activity of metal alloys, the TMC and TMN cores modulate the binding energies of alkynes and alkenes on Pt surfaces to achieve high selectivity toward partial alkyne hydrogenation mainly by an electronic effect. DFT and X-ray absorption spectroscopy (XAS) demonstrate a down-shift of the Pt d-band center, implicating changes in the electronic structure as the cause for the weakened adsorption of the C_2H_4. This effect was further confirmed by microcalorimetry measurements coupled with reactivity studies under industrial front end conditions. The altered binding energy of the core−shell catalysts resulted in drastically higher selectivity values when compared to a control Pt catalyst. Ultimately, an optimized 1 ML Pt/TiWN catalyst achieved net ethylene generation during simulated front-end industrial reaction conditions featuring C_2H_2 in a large excess of C_2H_4 and H_2.

RESULTS AND DISCUSSION

The partial hydrogenation of pure acetylene was investigated as a function of Pt shell coverage and core composition in order to gain insight into reactivity trends. Given the aim of this work is to demonstrate the impact that the changes in the electronic structure of Pt have on selectivity in a series reaction, a commercial catalyst composed of Pt nanoparticles supported on carbon was used for comparison. The materials studied comprised nominal Pt shell coverages of 0.5, 1, and 2 ML over TiWC and TiWN cores (synthetic and characterization details found in the Supporting Information and references; more detailed characterization studies confirming the core−shell structure before reaction can be found in our previous work).[20,21] Although all samples feature some degree of imperfect shell coverage, on average, materials with lower nominal Pt loadings tended to have a greater extent of the exposed core compared to core−shell catalyst samples with a greater content of Pt as indicated by scanning transmission electron microscopy (STEM) imaging and energy-dispersive X-ray spectroscopy (EDS) mapping.[18] Importantly, the core−shell structure remained intact after the reaction, as confirmed by STEM-EDS mapping shown in the Figure S1. Additionally, the PXRD patterns (Figure S2) and XPS spectra (Figure S3) collected before and after reaction suggest the core−shell architecture remained unaltered. These results are expected given the core−shell structure is assembled at high temperatures under hydrocarbon/H_2 atmospheres and remains stable under recarburization conditions (600 °C, 80% CH_4, 20% H_2) as confirmed by in situ extended X-ray absorption fine structure (EXAFS) analyses.[19] C_2H_4 and C_2H_6 were the main hydrogenation products, with minimal contribution of C_2^+ species to the overall carbon balance. As shown in Figure 1a and Figure S4, for all Pt coverages and core materials studied, we observed significant improvements in C_2H_4 selectivity compared to a commercial 5 wt % carbon-supported Pt catalyst (Premetek). Specifically, core−shell materials generated C_2H_4 selectivity values ranging from 60 to 80% across a range of shell coverages and temperatures while the commercial Pt catalyst was ~20% regardless of acetylene conversion level (i.e., either 5% or 71%, Figure 1a, Figure S4). These values compared favorably to C_2H_4 selectivity values obtained with state-of-the-art Pd-based catalysts, albeit under slightly different experimental conditions.[30] Interestingly, the Pt coverage did not significantly affect the C_2H_4 selectivity while the core composition did, with Pt/TiWN materials reaching 77% C_2H_4 selectivity compared to the 60% obtained with Pt/TiWC. Due to the wide range of activities across samples, the reaction temperature was varied between 345−388 K in order to compare C_2H_4 selectivity values at near

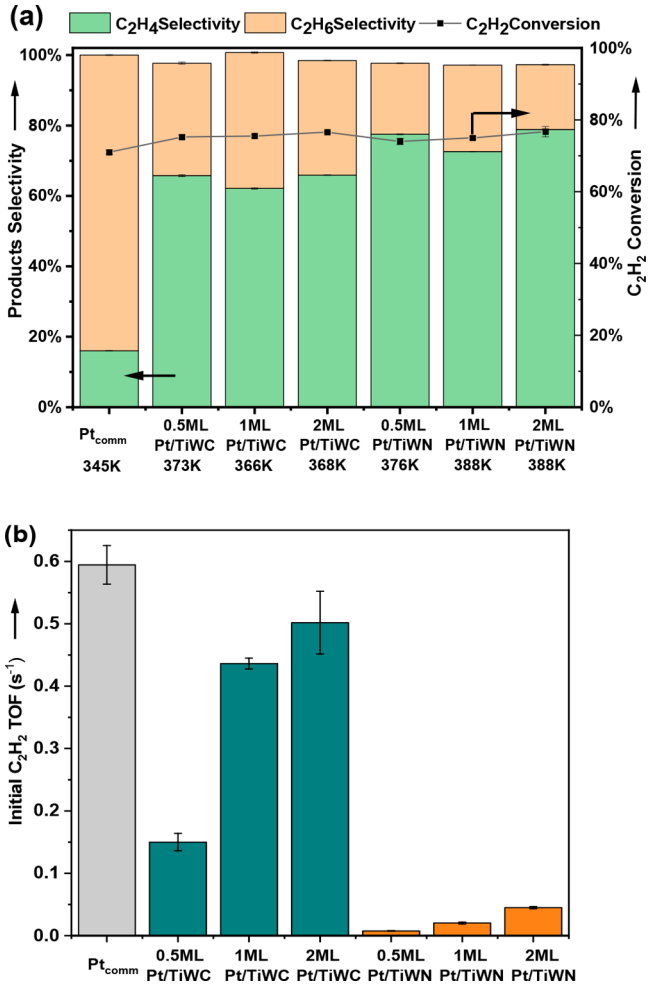

Figure 1. C_2H_2 hydrogenation results over different Pt-based catalysts. (a) Selectivity and conversion values measured at different temperatures to achieve ~75% conversion; (b) turnover frequency of C_2H_2 hydrogenation collected at differential conditions and constant temperature (reaction conditions for Figure 1b, constant temperature at 353 K, C_2H_2= 0.05 atm, H_2 = 0.20 atm, CH_4 = 0.08 atm internal standard, and He = 0.67 atm with a gas hourly space velocity (GHSV) ~ 1800 h^{-1}). Error bar indicated the propagated error (standard deviation during the number of site measurements and reactivity).

https://dx.doi.org/10.1021/acscatal.9b04070
ACS Catal. 2020, 10, 6763−6770

isoconversion levels. C_2H_4 selectivity for core−shell particles was independent of acetylene conversion for data collected at either different space velocity or reaction temperature. Conversely, Pt_{comm} featured higher C_2H_4 selectivity at higher temperatures (see Figures S5−S7), likely because acetylene outcompetes ethylene for adsorption sites at these conditions.[29] The reaction likely follows the Horiuti−Polanyi mechanism with a strong acetylene adsorption step, in agreement with the kinetic analysis by Vincent et al.[31]

The activity, quantified by the turnover frequency (TOF, defined as C_2H_2 molecules consumed per surface Pt atom per second), varied significantly with Pt coverage and choice of core material (Figure 1b). The rates were calculated under differential conditions at a reaction temperature of 353 K in the absence of mass transfer limitations and were normalized by the number of Pt surface sites as quantified by hydrogen underpotential deposition (Hupd) (see the Supporting Information for more details). Neither the bare TiWC nor TiWN cores were active for acetylene hydrogenation under these conditions (Figure S4c). For submonolayer Pt coverage, note that the Hupd method does not count exposed core sites, as shown in Table S3.[20,21] We observed similar acetylene hydrogenation rates on the 1 and 2 ML samples, while 0.5 ML samples featured much lower TOF values. These results suggest contiguous surface Pt atoms are more reactive than Pt-core interfacial sites. It appears that increasing core coverage had a positive effect on TOF without jeopardizing selectivity; the origin of this effect is currently unknown. The core material also drastically affected C_2H_2 TOF values: Pt/TiWN exhibited 10−70 times lower TOF values than Pt_{comm}, while Pt/TiWC only exhibited 1.2−3.5 times lower activity, which is consistent with activity-selectivity trade-offs in bulk metals and alloys that result from scaling relations between adsorbate binding energies.[24] The reactivity difference among Pt_{comm}, Pt/TiWC, and Pt/TiWN exemplifies the strong influence of the core material on the activity and reaction kinetics of the Pt shell. Since hydrogenation of C_2H_2 is a structure-insensitive reaction,[32−34] the observed altered reaction rates and product selectivity cannot be ascribed to changes in catalyst morphology or size. Den Hartog et al. reported similar C_2H_4 selectivity for acetylene hydrogenation over Pt nanoparticles with sizes ranging from 2 to 20 nm.[34] In addition, our previous study indicated the Pt−Pt coordination numbers and Pt−Pt distances are very similar for Pt_{comm} and 2 ML core−shell particles reduced in H_2 at 573 K (shown in Table S4).[19]

We compared the hydrogenation activity of Pt_{comm} and the core−shell nanoparticles using a C_2H_4 feed (full experimental details in the Supporting Information) to assess if our catalysts could be used under industrial acetylene hydrogenation conditions in which C_2H_2 has to be hydrogenated in an excess of C_2H_4. The TOF values for C_2H_4 hydrogenation decreased in the order Pt_{comm} > Pt/TiWC > Pt/TiWN (Figure S8). Importantly, all catalysts featured C_2H_4 hydrogenation rates nearly an order of magnitude faster than those measured for C_2H_2, which immediately poses a selectivity challenge for industrial C_2H_2 hydrogenation conditions unless there are drastic differences in adsorption strength on the catalyst surface between these molecules. We, therefore, investigated the effects of adsorbate binding energies on reaction rates and selectivity as a function of the catalyst composition. Microcalorimetry measurements showed markedly different results during the adsorption of C_2H_4 and C_2H_2 on the core−shell catalysts as compared to Pt_{comm} shown in Table 1. The Pt-normalized uptake of C_2H_2 and C_2H_4 on 2 ML Pt/TiWC and 2 ML Pt/TiWN were more than an order of magnitude reduced compared to Pt_{comm}, which is surprising given that Hupd measurements showed a similar number of active sites for the materials (Table S3). This difference suggests drastic changes in heat of adsorption of C_2H_2 and C_2H_4 on the core−shell particles compared to Pt_{comm}. Given that our microcalorimeter features a measurement limit of ∼20 kJ mol^{-1}, these data suggest that a small amount of C_2H_2 binds strongly to a few sites and that most of the C_2H_2 is bound to the core−shell surface so weakly that it could not be captured by the microcalorimetry measurement. More significantly, the ratios of adsorbed C_2H_2 to C_2H_4 increased in the order Pt_{comm} < Pt/TiWC < Pt/TiWN, in agreement with the observed selectivity trend. Indeed, the heat of adsorption (ΔH_{ads}) measurements showed marked differences across samples. At 298 K, the ΔH_{ads} for C_2H_2 and C_2H_4 on Pt_{comm} was 200 kJ mol^{-1} and 190 kJ mol^{-1}, respectively, consistent with literature values.[29,35−37] The maximum uncertainty in the calorimetry measurements is estimated to be 10 kJ mol^{-1} through previous experiments with a similar setup.[38] In stark contrast, C_2H_4 adsorption on the core−shell nanoparticles was much less exothermic, measuring 125 kJ mol^{-1} for 2 ML Pt/TiWC and below instrumental detection limits (∼20 kJ mol^{-1}) for 2 ML Pt/TiWN as would be expected from the differences in amounts of C_2H_4 adsorption and reactivity trends. Although C_2H_2 appeared to adsorb more strongly on the core−shell nanoparticles than on Pt_{comm} (260−290 kJ mol^{-1} vs 200 kJ mol^{-1}), the number of adsorbed C_2H_2 molecules was an order of magnitude lower. In Table S3, the reduced number of adsorbed C_2H_2 was not due to fewer available Pt exposed sites, given that the dispersion is similar between the core−shell carbide, nitride and commercial Pt catalysts (as measured by hydrogen underpotential deposition in Table S3). These results can possibly be reconciled by acetylene dehydrogenation. The experimental procedure adopted for the microcalorimetry measurements without a H_2 cofeed could have overestimated the C_2H_2 ΔH_{ads} value due to the exothermicity of initial coke formation via C_2H_2 dehydrogenation upon adsorption.[29,39,40] Regardless, the measured difference in binding for the alkyne and the olefin is consistent with the reactivity trends.

We performed XAS and XPS measurements to gain insight into the electronic structure changes between Pt_{comm} and the Pt in the core−shell materials. A Pt L_2 edge (13.27 keV) spectrum was taken rather than Pt L_3 edge (11.56 keV) due to overlap with the W L_2 edge (11.54 keV). X-ray absorption near edge structure (XANES) experiments showed greater white line intensities for Pt/TiWN than for Pt/TiWC, while the Pt foil showed almost no white line features (Figure 2). Given the

Table 1. Microcalorimetry Data for Core−Shell Particles and Pt_{comm}

	Pt_{comm}	2 ML Pt/TiWC	2 ML Pt/TiWN
C_2H_2 adsorption amount (mol C_2H_2/mol Pt site)	>0.206	0.006	0.018
C_2H_4 adsorption amount (mol C_2H_4/mol Pt site)	0.109	0.002	0
C_2H_2 H_{ads} (kJ mol^{-1})	−200	−260	−290
C_2H_4 H_{ads} (kJ mol^{-1})	−190	−125	N.A.[a]

[a]Adsorption of C_2H_4 at room temperature was below instrumental detection limits (indicating the absolute value of the heat of adsorption was less than ∼20 kJ mol^{-1}).

https://dx.doi.org/10.1021/acscatal.9b04070
ACS Catal. 2020, 10, 6763−6770

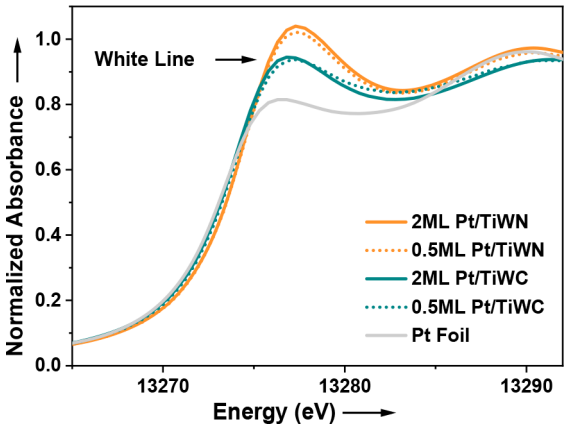

Figure 2. XANES of Pt and core−shell Pt, Pt foil, and Pt core−shell L_2 edge (13.27 keV) XANES spectra. Pt L_3 edge (11.56 keV) spectrum was not taken due to overlap with the W L_2 edge (11.54 keV).

samples are fully reduced and do not feature significant Pt−O bonding as measured by extended X-ray absorption fine structure (EXAFS) (Table S5), these data indicate a change in the electronic structure of metallic Pt resulting from d-band broadening accompanied by a down-shift of the d-band center, as further confirmed by Garg et al. with detailed follow-up in situ characterization studies.[19] In addition, Table S5 also demonstrates the Pt−Pt bond distances are within 0.03 Å across bulk and core−shell samples, which indicates the cores do not induce a strong strain effect. XPS was used to characterize the formation of the core−shell nanoparticles following prior analysis protocols.[21] The Pt $4f_{7/2}$ peaks for Pt/TiWN and TiWC (71.8 and 71.5 eV, respectively) were centered at higher energies than those of metallic Pt (71.2 eV) (Figure S7c), an effect known to correlate with the down-shifting of the d-band center.[1,21,41,42]

A similar Pd $3d_{5/2}$ core-level shift was reported in the Pd catalyst for alkyne hydrogenation that was associated with the creation of a Pd−C surface phase.[43] However, such phenomenon was observed in our system as the Pt $4f_{7/2}$ core-level shift for the core−shell particles that existed prior to feeding the reactant gases and remained in the same position after the reaction, as shown in the Figure S3. In addition, unlike Pd, the formation of Pt carbide is thermodynamically unfavorable under our reaction conditions.[44] Furthermore, our previous DFT calculation showed interactions between Pt−W are much more energetically favored than the Pt−C interaction, which rules out the formation of PtC_x species during the reaction.[20] The XPS data show that the Pt in the shell and the W in the core had reverse core electron binding energy shifts, indicative of strong Pt−W bonding interactions and in agreement with prior studies on this system.[21] The core-hole/final state effects have little influence on the observed binding energy shift. Therefore, these results are strong evidence the carbide and nitride cores significantly alter the electronic structure of the Pt overlayers.

DFT calculations confirmed the experimentally observed differences in adsorption energies and electronic structures among Pt_{comm} and the core−shell nanoparticles. The binding energies of C_2H_2 and C_2H_4 on the core−shell materials are nearly 1 eV weaker compared to Pt(111) (Table S6). This result is consistent with the drastic differences in achievable total C_2H_x coverages on Pt/TiWC and Pt/TiWN compared to Pt_{comm} shown in Table 1. Indeed, experimental measurements directly probe the adsorption energy of reactive sites, but averaging the heats of adsorption over all sites, most of which do not adsorb C_2H_2 or C_2H_4, would produce similar results as those predicted by DFT. Notably, the C_2H_2 TOF has the trend of Pt > Pt/TiWC > Pt/TiWN, which is consistent with activity-selectivity trade-offs in bulk metals and alloys resulting from scaling relations between adsorbate binding energies.[24] In addition, the integral binding energies (IBEs) of the second Pt layer were positive for both Pt/TiWC and Pt/TiWN core−shells at 0.035 eV/Å^2 and 0.016 eV/ Å^2, respectively, which indicated the second Pt 2D-layer is less stable relative to 3D Pt growth (see the Supporting Information for details). Hence the 1 ML Pt/TiWC and Pt/TiWN models were chosen to compare with the experimental data.

Analysis of the d-band structure showed the Pt d-band center energy, relative to the Fermi level, changed from −1.97 eV for the Pt(111) surface to −2.82 eV for 1 ML Pt/TiWC and −2.95 eV for 1 ML Pt/TiWN (Table S7). Prior reports on early transition metal nitride @Pt core−shell structures for the oxygen reduction reaction similarly featured downshifted d-band centers that affected the binding energy of surface oxygen species.[45,46] In light of these results, we investigated the C_2H_2 hydrogenation pathway through DFT calculations over Pt(111), 1 ML Pt/TiWC, and 1 ML Pt/TiWN surfaces. We calculated adsorption energies on multiple hollow, bridge, and atop sites and selected the strongest adsorption configuration from which to determine C_2H_2 hydrogenation barriers. Specifically, C_2H_2 adsorbed in a hollow site was chosen for both Pt(111) and core−shell particles; the C_2H_4 atop site configuration was chosen for core−shell particles; and the bridge site configuration was chosen for Pt(111). As shown in Figure 3, the energy profile for C_2H_2 hydrogenation over 1 ML

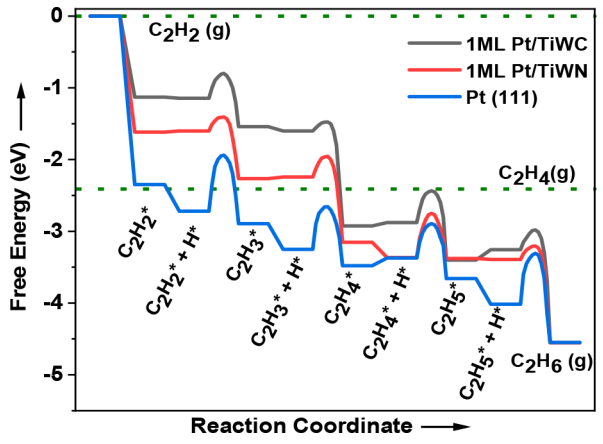

Figure 3. C_2H_2 hydrogenation energy diagram: 1 ML Pt/TiWC (black), 1 ML Pt/TiWN (red), and Pt (111) (blue).

Pt/TiWC and 1 ML Pt/TiWN indicates that both surfaces are highly active to C_2H_2 hydrogenation, with activation barriers of 0.35 and 0.19 eV, respectively. Notably, the C_2H_4 hydrogenation barrier on Pt(111) is significantly lower than the desorption energy, with a 0.35 eV difference, indicating high activity of Pt(111) for C_2H_4 hydrogenation. In contrast, the C_2H_4 hydrogenation barriers on the core−shell structure are comparable to the desorption energies (0.07 eV of difference for 1 ML Pt/TiWC and 0.12 eV of difference for 1 ML Pt/TiWN), implying these materials should exhibit better C_2H_4 selectivity than Pt(111). The difference between C_2H_4

https://dx.doi.org/10.1021/acscatal.9b04070
ACS Catal. 2020, 10, 6763−6770

desorption energy and further hydrogenation to the C_2H_5 barrier has been used to predict ethylene selectivity.[24] From the DFT perspective, it is difficult to predict overall selectivity differences between the 1 ML Pt/TiWC and 1 ML Pt/TiWN surfaces, as each surface Pt atom is not identical to each other considering the local subsurface environment and each has different ethylene desorption and activation energies. C_2H_4 adsorption is significantly weakened on the core−shell structures, which is the key factor for improving C_2H_4 selectivity.[24] The hydrogenation energetics in Figure 3 were based on the strongest adsorption configuration; Pt/TiWN has stronger $*C_2H_2$ binding energy than the Pt/TiWC, yet other stable adsorption configurations could contribute to the observed difference in the acetylene TOF data in Figure 1b between Pt/TiWN and Pt/TiWC. Additionally, differences in reaction rates could also arise from differences in H_2 binding energies. As it can be seen in Figure 3, for the $C_2H_2^* + H^*$ step, both Pt/TiWC and Pt decreased in total free energy from the previous step which indicated the H_2 adsorption was favored on Pt/TiWC and Pt. However, for Pt/TiWN, the $C_2H_2^* + H^*$ total free energy increased from the $C_2H_2^*$ step, which indicated H_2 adsorption to the Pt/TiWN surface was unfavorable and hence limited C_2H_2 turnover frequency on Pt/TiWN as shown in Figure 1b.

Inspired by the promising results on pure feeds, we investigated C_2H_2 partial hydrogenation under industrially relevant conditions.[47,48] Simulating front-end conditions, we performed test reactions with a $C_2H_2/C_2H_4/H_2$ ratio of 1:20:15, a gas hourly space velocity (GHSV) ~ 1800 h^{-1} at ambient pressure under and temperatures ranging from 348 to 378 K to maintain isoconversion of C_2H_2 (80%) (see the Supporting Information for full experimental details). Note that catalyst performance can be assessed by tracking C_2H_4 consumption, but a selective catalyst that generates more C_2H_4 that it consumed would result in a "negative" C_2H_4 conversion value when using the traditional definition of conversion (eq 1).

$$C_2H_4 \text{ conversion} = \frac{C_2H_{4(\text{feed})} - C_2H_{4(\text{effluent})}}{C_2H_{4(\text{feed})}} \quad (1)$$

As shown in Table 2, Pt_{comm} had the highest C_2H_4 consumption values of ~16% of the feed, followed by Pt/TiWC (~5% of the feed) and finally Pt/TiWN (~0−2% of the feed). The 1 ML Pt/TiWN demonstrated a modest net generation of C_2H_4 (i.e., a −0.3% C_2H_4 conversion) under these conditions. As the core−shell nitride nanoparticles demonstrated less C_2H_4 consumption at ~80% C_2H_2 conversion, C_2H_4 disappearance was further measured at a C_2H_2 conversion of ~95%, as shown in Table S8. As shown in Figure S9, 1 ML Pt/TiWN featured high stability with no activity decay for more than 10 h at acetylene conversion levels with a turnover number of 22400 that was comparable to that obtained with Pt_{comm} under similar conditions. The 1 ML Pt/TiWN featured higher C_2H_4 selectivity than the 0.5 ML Pt/TiWN material. In our prior DFT study[49] focusing on the effect of Pt coverage over early transition metal carbide underlayers, we showed that a 1 ML had a lower d-band center than a 0.75 ML for the Pt/TiWC system. Therefore, lower Pt loadings were not pursued in the present study.

Table 2. Front-End Condition Core−Shell Particles and Pt_{comm} Reactivity[a]

	temperature (K)	C_2H_2 conversion (%)	C_2H_4 conversion (%)
Pt_{comm}	371	83.1	15.9 ± 0.2
1 ML Pt/TiWC	354	81.5	5.4 ± 0.1
2 ML Pt/TiWC	348	82.1	5.0 ± 0.1
0.5 ML Pt/TiWC	353	81.5	4.7 ± 0.2
2 ML Pt/TiWN	378	85.9	2.1 ± 0.1
0.5 ML Pt/TiWN	378	81.4	1.0 ± 0.1
1 ML Pt/TiWN	368	83.0	−0.3 ± 0.1[b]

[a] C_2H_2 = 0.02 atm, H_2 = 0.23 atm, C_2H_4 = 0.31 atm, CH_4 = 0.15 atm (internal standard), and He = 0.29 atm with a gas hourly space velocity (GHSV) ~ 1800 h^{-1}. [b] A negative C_2H_4 conversion meant that there was C_2H_4 net generation.

In order to understand the origin of C_2H_6 overhydrogenated products as related to the intrinsic and net ethylene selectivity, defined in eqs 2 and 3 below, we performed hydrogenation experiments in a recirculating batch reactor with isotopically labeled $^{13}C_2H_4$ and $^{12}C_2H_2$ to track specific $^{12}C_2H_4$, $^{12}C_2H_6$, and $^{13}C_2H_6$ generation for the 1 ML Pt/TiWN catalyst (detailed setup in the Supporting Information).[50,51]

$$\text{intrinsic } C_2H_4 \text{ selectivity} = \frac{^{12}C_2H_4}{\Delta\,^{12}C_2H_2} \quad (2)$$

$$\text{net } C_2H_4 \text{ selectivity} = \frac{^{12}C_2H_4 - {}^{13}C_2H_6}{\Delta\,^{12}C_2H_2} \quad (3)$$

A batch reactor was charged initially with 6 Torr $^{12}C_2H_2$, 120 Torr $^{13}C_2H_4$, and 90 Torr H_2 to maintain a similar $C_2H_2/C_2H_4/H_2$ = 1:20:15 ratio to that used in the flow reactor front-end conditions. The net C_2H_4 selectivity defined in eq 3 was positive as shown in Figure 4a, which is consistent with a net

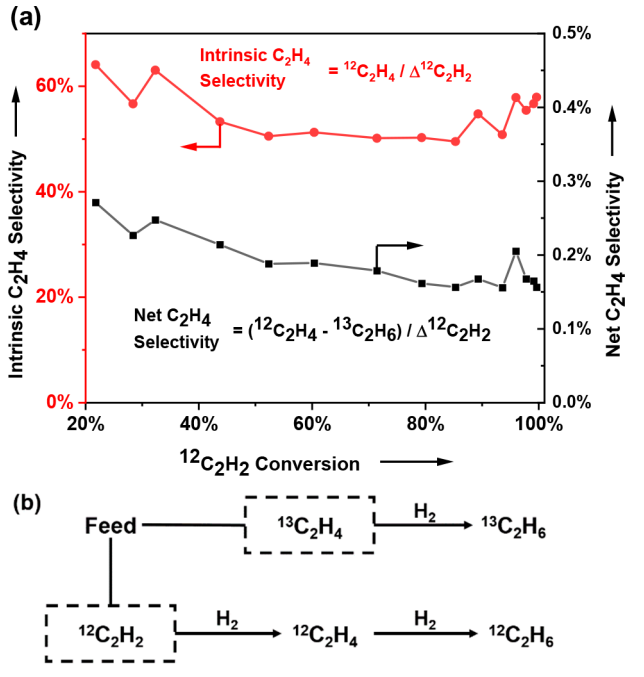

Figure 4. Isotopic study of C_2H_4 selectivity vs C_2H_2 conversion and reaction network schematic. (a) Variation of intrinsic $^{12}C_2H_4$ selectivity and net C_2H_4 selectivity (see the formula for definitions) with the $^{12}C_2H_2$ conversion (*x*-axis) are illustrated by red and black lines, respectively. (b) Schematics of the isotopic study.

https://dx.doi.org/10.1021/acscatal.9b04070
ACS Catal. 2020, 10, 6763−6770

generation of C_2H_4 observed under the flow reactor industrial conditions. Based on the definition of eqs 2 and 3 and the data shown in Figure 4a, we calculated that ~88% C_2H_6 was generated from the hydrogenation of $^{13}C_2H_4$. Thus, for the unwanted overhydrogenation, $^{13}C_2H_6$ formation was from the hydrogenation of $^{13}C_2H_4$ rather than from the sequential hydrogenation of bound $^{12}C_2H_2$ intermediates.

CONCLUSIONS

Through a combination of reactivity, characterization, and computational studies, we demonstrated the Pt electronic structure was modified by interactions with the underlying transition metal carbide or nitride core, leading to a modulation of the relative adsorption energies of C_2H_2 and C_2H_4 and a remarkable enhancement in C_2H_4 selectivity in the industrially important hydrogenation of C_2H_2. More generally, our core−shell nanoparticle platform represents a general means by which the electronic properties of noble metals can be tuned for the enhancement of their catalytic properties. These results motivate further exploration of accessible combinations of shell coverages and core materials to control reactivity and selectivity for a wide range of reactions while also unearthing structure−property relationships that extend our fundamental understanding of core−shell nanoparticle catalysis.

EXPERIMENTAL SECTION

A comprehensive description of the experimental methods is documented in the Supporting Information.

Sample Preparation. Core−shell carbide particles were synthesized through carburizing mixtures of H_2PtCl_6 and tungsten oxides encapsulated in removable silica templates.[20] Core−shell nitride samples were obtained through nitridation of the core−shell carbide sample.[21] Platinum nanoparticles supported on tungsten carbide were synthesized through the incipient wetness impregnation (IWI) method, and commercial Pt on carbon black was purchased from Premetek. Inc.

Catalytic Reactions. Catalytic reactions were performed in a single-pass-plug-flow reactor. Catalyst (~2−70 mg) was well mixed with α-alumina (4.0 g, 100−200 mesh) to enhance heat transfer. The reactor temperature was kept constant with an ATS furnace. For the acetylene hydrogenation reaction, the total flow rate was 60 mL/min (C_2H_2 = 3 mL/min, H_2 = 12 mL/min, CH_4 = 5 mL/min (internal standard), He = 40 mL/min or C_2H_2 = 0.05 atm, H_2 = 0.20 atm, CH_4 = 0.08 atm (internal standard), and He = 0.67 atm) at 1 atm with a gas hourly space velocity (GHSV) of 1800 h^{-1}, reaction temperature was varied from 343 to 388 K. For acetylene hydrogenation at industrial conditions, the total flow rate was 65 mL/min (5% C_2H_2/He = 20 mL/min, H_2 = 15 mL/min, C_2H_4 = 20 mL/min CH_4 = 10 mL/min (internal standard) or C_2H_2 = 0.02 atm, H_2 = 0.23 atm, C_2H_4 = 0.31 atm CH_4 = 0.15 atm (internal standard) and He = 0.29 atm), and the reaction temperature was varied from 348 to 378 K. For C_2H_4 hydrogenation, the total flow rate was 60 mL/min (C_2H_4 = 5 mL/min, H_2 = 5 mL/min, CH_4 = 5 mL/min, He = 45 mL/min or C_2H_4 = 0.08 atm, H_2 = 0.08 atm, CH_4 = 0.08 atm (internal standard) and He = 0.75 atm), and the reaction temperature was set to be 318 K. The product distribution was analyzed by an Agilent 6890 FID gas chromatograph. Industrial reaction conditions with cofed $^{13}C_2H_4$ and $^{12}C_2H_2$ was carried out in a batch reactor equipped with a pump to recirculate the reactant gases within the reactor. The effluent was analyzed with a Shimadzu QP 2010 Ultra GC-MS fitted with an Rt-Alumina BOND/KCl column. The system was free of heat and mass transfer limitations analyzed with Mear's and Weisz-Prater's criteria (shown in the Supporting Information).[52,53]

Sample Characterization. Nanoparticle particle sizes before and after reaction were measured with transmission electron microscopy (TEM, JEOL 2010) with a field emission gun (FEG) operating at 200 kV. Crystal structures before and after reaction were measured by powder X-ray diffraction (PXRD, Bruker D8) using a Cu Kα radiation source. Pt, Ti, and W contents were measured by inductively coupled plasma-mass spectrometry (ICP-MS, Agilent 7900) and thermogravimetric analysis (TGA, TA-Q500). The number of sites for the control Pt_{comm} catalyst was measured electrochemically through the H_{upd} method and the conventional CO chemisorption while core−shell particles were measured only electrochemically. Microcalorimetry was carried out in a combined homemade breakthrough reactor (BTR)-differential scanning calorimetry (DSC)-mass spectrometer (MS) instrument. Ex-situ X-ray absorption fine structure (XAFS, APS, Argonne National Lab, Pt L_2-edge 13 273 eV) was measured for core−shell samples, Pt foil, and PtO_2. A PHI Versaprobe II spectrometer with a monochromatic aluminum anode X-ray source was used to perform the photoemission spectra before and after reaction to analyze the catalyst surface composition.

DFT Calculation. Electronic structure calculations were performed using the Vienna ab initio simulation package (VASP).[54] The projector augmented-wave (PAW) method was used to represent the ion−core electron interactions.[55] Nonlocal gradient corrections to the total energy were calculated using the Perdew−Burke−Ernzerhof revised for the solid (PBE sol) exchange correlation functional.[56] The heat, quench, and exfoliation (HQE) method was used to construct the core−shell model.[49] A detailed description of the construction of the Pt overlayer model, including analysis of the optimal Pt density and stability in the monolayer structure, is included in the Supporting Information.

Code Availability. The corresponding codes for the density functional theory calculations are available upon request.

ASSOCIATED CONTENT

Supporting Information

The Supporting Information is available free of charge at https://pubs.acs.org/doi/10.1021/acscatal.9b04070.

Additional materials characterization; ethylene selectivity at different temperatures and conversions; kinetics data; DFT model calculation, d-band center; core−shell stability results; reactor setup; catalysts synthesis; microcalorimetry measurements; isotopic-labeled reaction results; and mass/heat transfer limitation calculation (PDF)

AUTHOR INFORMATION

Corresponding Authors

Yuriy Román-Leshkov − *Department of Chemical Engineering, Massachusetts Institute of Technology, Cambridge, Massachusetts 02139, United States;* orcid.org/0000-0002-0025-4233; Email: yroman@mit.edu

https://dx.doi.org/10.1021/acscatal.9b04070
ACS Catal. 2020, 10, 6763−6770

Robert M. Rioux − *Department of Chemical Engineering and Department of Chemistry, The Pennsylvania State University, University Park, Pennsylvania 16802, United States;* orcid.org/0000-0002-6019-0032; Email: rioux@engr.psu.edu

Authors

Zhenshu Wang − *Department of Chemical Engineering, Massachusetts Institute of Technology, Cambridge, Massachusetts 02139, United States*

Aaron Garg − *Department of Chemical Engineering, Massachusetts Institute of Technology, Cambridge, Massachusetts 02139, United States*

Linxi Wang − *Department of Chemical Engineering, The Pennsylvania State University, University Park, Pennsylvania 16802, United States*

Haoran He − *Department of Chemical Engineering, The Pennsylvania State University, University Park, Pennsylvania 16802, United States*

Anish Dasgupta − *Department of Chemical Engineering, The Pennsylvania State University, University Park, Pennsylvania 16802, United States*

Daniela Zanchet − *Institute of Chemistry, University of Campinas, Campinas, São Paulo 13083-970, Brazil;* orcid.org/0000-0003-1475-2548

Michael J. Janik − *Department of Chemical Engineering, The Pennsylvania State University, University Park, Pennsylvania 16802, United States;* orcid.org/0000-0001-9975-0650

Complete contact information is available at: https://pubs.acs.org/10.1021/acscatal.9b04070

Notes

The authors declare no competing financial interest.

■ ACKNOWLEDGMENTS

Z.W. and Y.R.-L. acknowledge support by the U.S. Department of Energy, Office of Basic Energy Sciences under Award No. DE-SC0016214. L.W., A.D., and R.M.R. acknowledge the Department of Energy, Office of Basic Energy Sciences, Chemical Sciences, Geosciences and Biosciences Division, Catalysis Sciences Program (Grant No. DE-SC0016192) for support of this research. H.H. and J.M.J acknowledge the US National Science Foundation (NSF grant # CBET−1748365) for financial support of this work. H.H. acknowledges training provided by the Computational Materials Education and Training (CoMET) NSF Research Traineeship (Grant No. DGE-1449785). This work used the Extreme Science and Engineering Discovery Environment (XSEDE), which is supported by the National Science Foundation under Grant No. ACI-1548562. This research also used resources of the Advanced Photon Source, a U.S. DOE, Office of Science User Facility operated for the DOE office of Sceince by Argonne National Laboratory under Contract No. De-AC0206CH11357 (12-BM-B beamline, GUP 55290). Z.W. thanks the Chyn Duog Shiah Memorial Fellowship for financial support. We thank Dr. Mark M. Sullivan for fruitful discussions.

■ REFERENCES

(1) Alayoglu, S.; Nilekar, A. U.; Mavrikakis, M.; Eichhorn, B. Ru-Pt Core-Shell Nanoparticles for Preferential Oxidation of Carbon Monoxide in Hydrogen. *Nat. Mater.* **2008**, *7*, 333−338.

(2) Tauster, S. J.; Fung, S. C.; Baker, R. T. K.; Horsley, J. A. Strong-Interactions in Supported-Metal Catalysts. *Science* **1981**, *211*, 1121−1125.

(3) Shao, M. H.; Peles, A.; Shoemaker, K. Electrocatalysis on Platinum Nanoparticles: Particle Size Effect on Oxygen Reduction Reaction Activity. *Nano Lett.* **2011**, *11*, 3714−3719.

(4) Qiao, B. T.; Wang, A. Q.; Yang, X. F.; Allard, L. F.; Jiang, Z.; Cui, Y. T.; Liu, J. Y.; Li, J.; Zhang, T. Single-Atom Catalysis of CO Oxidation Using Pt_1/FeO_x. *Nat. Chem.* **2011**, *3*, 634−641.

(5) Bratlie, K. M.; Lee, H.; Komvopoulos, K.; Yang, P. D.; Somorjai, G. A. Platinum Nanoparticle Shape Effects on Benzene Hydrogenation Selectivity. *Nano Lett.* **2007**, *7*, 3097−3101.

(6) Narayanan, R.; El-Sayed, M. A. Shape-Dependent Catalytic Activity of Platinum Nanoparticles in Colloidal Solution. *Nano Lett.* **2004**, *4*, 1343−1348.

(7) Cheng, N. C.; Stambula, S.; Wang, D.; Banis, M. N.; Liu, J.; Riese, A.; Xiao, B. W.; Li, R. Y.; Sham, T. K.; Liu, L. M.; Botton, G. A.; Sun, X. L. Platinum Single-Atom and Cluster Catalysis of the Hydrogen Evolution Reaction. *Nat. Commun.* **2016**, *7*, 13638.

(8) Cui, X. J.; Li, W.; Ryabchuk, P.; Junge, K.; Beller, M. Bridging Homogeneous and Heterogeneous Catalysis by Heterogeneous Single-Metal-Site Catalysts. *Nat. Catal* **2018**, *1*, 385−397.

(9) O'Connor, N. J.; Jonayat, A. S. M.; Janik, M. J.; Senftle, T. P. Interaction Trends between Single Metal Atoms and Oxide Supports Identified with Density Functional Theory and Statistical Learning. *Nat. Catal* **2018**, *1*, 531−539.

(10) Roy, C.; Sebok, B.; Scott, S. B.; Fiordaliso, E. M.; Sorensen, J. E.; Bodin, A.; Trimarco, D. B.; Damsgaard, C. D.; Vesborg, P. C. K.; Hansen, O.; Stephens, I. E. L.; Kibsgaard, J.; Chorkendorff, I. Impact of Nanoparticle Size and Lattice Oxygen on Water Oxidation on $NiFeO_xH_y$. *Nat. Catal* **2018**, *1*, 820−829.

(11) Sasaki, K.; Naohara, H.; Cai, Y.; Choi, Y. M.; Liu, P.; Vukmirovic, M. B.; Wang, J. X.; Adzic, R. R. Core-Protected Platinum Monolayer Shell High-Stability Electrocatalysts for Fuel-Cell Cathodes. *Angew. Chem., Int. Ed.* **2010**, *49*, 8602−8607.

(12) Strasser, P.; Koh, S.; Anniyev, T.; Greeley, J.; More, K.; Yu, C. F.; Liu, Z. C.; Kaya, S.; Nordlund, D.; Ogasawara, H.; Toney, M. F.; Nilsson, A. Lattice-Strain Control of the Activity in Dealloyed Core-Shell Fuel Cell Catalysts. *Nat. Chem.* **2010**, *2*, 454−460.

(13) Wanjala, B. N.; Luo, J.; Loukrakpam, R.; Fang, B.; Mott, D.; Njoki, P. N.; Engelhard, M.; Naslund, H. R.; Wu, J. K.; Wang, L. C.; Malis, O.; Zhong, C. J. Nanoscale Alloying, Phase-Segregation, and Core-Shell Evolution of Gold-Platinum Nanoparticles and Their Electrocatalytic Effect on Oxygen Reduction Reaction. *Chem. Mater.* **2010**, *22*, 4282−4294.

(14) Wang, X.; Choi, S. I.; Roling, L. T.; Luo, M.; Ma, C.; Zhang, L.; Chi, M. F.; Liu, J. Y.; Xie, Z. X.; Herron, J. A.; Mavrikakis, M.; Xia, Y. N. Palladium-Platinum Core-Shell Icosahedra with Substantially Enhanced Activity and Durability Towards Oxygen Reduction. *Nat. Commun.* **2015**, *6*, 7594.

(15) Jain, A.; Ramasubramaniam, A. Tuning Core-Shell Interactions in Tungsten Carbide-Pt Nanoparticles for the Hydrogen Evolution Reaction. *Phys. Chem. Chem. Phys.* **2018**, *20*, 23262−23271.

(16) Tao, F.; Grass, M. E.; Zhang, Y. W.; Butcher, D. R.; Renzas, J. R.; Liu, Z.; Chung, J. Y.; Mun, B. S.; Salmeron, M.; Somorjai, G. A. Reaction-Driven Restructuring of Rh-Pd and Pt-Pd Core-Shell Nanoparticles. *Science* **2008**, *322*, 932−934.

(17) Cui, C. H.; Gan, L.; Heggen, M.; Rudi, S.; Strasser, P. Compositional Segregation in Shaped Pt Alloy Nanoparticles and Their Structural Behaviour During Electrocatalysis. *Nat. Mater.* **2013**, *12*, 765−771.

(18) Göhl, D.; Garg, A.; Paciok, P.; Mayrhofer, K. J. J.; Heggen, M.; Shao-Horn, Y.; Dunin-Borkowski, R. E.; Román-Leshkov, Y.; Ledendecker, M. Engineering Stable Electrocatalysts by Synergistic Stabilization between Carbide Cores and Pt Shells. *Nat. Mater.* **2020**, *19*, 287−291.

(19) Garg, A.; Goncalves, D. S.; Liu, Y. S.; Wang, Z. S.; Wang, L. X.; Yoo, J. S.; Kolpak, A.; Rioux, R. M.; Zanchet, D.; Roman-Leshkov, Y. Impact of Transition Metal Carbide and Nitride Supports on the

Electronic Structure of Thin Platinum Overlayers. *ACS Catal.* **2019**, *9*, 7090−7098.
(20) Hunt, S. T.; Milina, M.; Alba-Rubio, A. C.; Hendon, C. H.; Dumesic, J. A.; Roman-Leshkov, Y. Self-Assembly of Noble Metal Monolayers on Transition Metal Carbide Nanoparticle Catalysts. *Science* **2016**, *352*, 974−978.
(21) Garg, A.; Milina, M.; Ball, M.; Zanchet, D.; Hunt, S. T.; Dumesic, J. A.; Roman-Leshkov, Y. Transition-Metal Nitride Core@ Noble-Metal Shell Nanoparticles as Highly CO Tolerant Catalysts. *Angew. Chem., Int. Ed.* **2017**, *56*, 8828−8833.
(22) Hunt, S. T.; Milina, M.; Wang, Z. S.; Roman-Leshkov, Y. Activating Earth-Abundant Electrocatalysts for Efficient, Low-Cost Hydrogen Evolution/Oxidation: Sub-Monolayer Platinum Coatings on Titanium Tungsten Carbide Nanoparticles. *Energy Environ. Sci.* **2016**, *9*, 3290−3301.
(23) Studt, F.; Abild-Pedersen, F.; Bligaard, T.; Sorensen, R. Z.; Christensen, C. H.; Norskov, J. K. On the Role of Surface Modifications of Palladium Catalysts in the Selective Hydrogenation of Acetylene. *Angew. Chem., Int. Ed.* **2008**, *47*, 9299−9302.
(24) Studt, F.; Abild-Pedersen, F.; Bligaard, T.; Sorensen, R. Z.; Christensen, C. H.; Norskov, J. K. Identification of Non-Precious Metal Alloy Catalysts for Selective Hydrogenation of Acetylene. *Science* **2008**, *320*, 1320−1322.
(25) Huang, D. C.; Chang, K. H.; Pong, W. F.; Tseng, P. K.; Hung, K. J.; Huang, W. F. Effect of Ag-Promotion on Pd Catalysts by Xanes. *Catal. Lett.* **1998**, *53*, 155−159.
(26) Armbruster, M.; Kovnir, K.; Behrens, M.; Teschner, D.; Grin, Y.; Schlogl, R. Pd-Ga Intermetallic Compounds as Highly Selective Semihydrogenation Catalysts. *J. Am. Chem. Soc.* **2010**, *132*, 14745−14747.
(27) Meyer, R. J.; Zhang, Q.; Kryczka, A.; Gomez, C.; Todorovic, R. Perturbation of Reactivity with Geometry: How Far Can We Go? *ACS Catal.* **2018**, *8*, 566−570.
(28) Abon, M.; Massardier, J.; Tardy, B.; Bertolini, J. C. Pt50ni50(111) Alloy and Pt(111) - Chemisorptive Properties for Acetylene and Ethylene and Catalytic Behavior for the Acetylene Selective Hydrogenation. *Surf. Sci.* **1987**, *189*, 880−885.
(29) Spiewak, B. E.; Cortright, R. D.; Dumesic, J. A. Microcalorimetric Studies of H_2, C_2H_4, and C_2H_2 Adsorption on Pt Powder. *J. Catal.* **1998**, *176*, 405−414.
(30) Osswald, J.; Kovnir, K.; Armbruster, M.; Giedigkeit, R.; Jentoft, R. E.; Wild, U.; Grin, Y.; Schlogl, R. Palladium-Gallium Intermetallic Compounds for the Selective Hydrogenation of Acetylene - Part II: Surface Characterization and Catalytic Performance. *J. Catal.* **2008**, *258*, 219−227.
(31) Vincent, M. J.; Gonzalez, R. D. A Langmuir-Hinshelwood Model for a Hydrogen Transfer Mechanism in the Selective Hydrogenation of Acetylene over a Pd/Gamma-Al_2O_3 Catalyst Prepared by the Sol-Gel Method. *Appl. Catal., A* **2001**, *217*, 143−156.
(32) Sheth, P. A.; Neurock, M.; Smith, C. M. First-Principles Analysis of the Effects of Alloying Pd with Ag for the Catalytic Hydrogenation of Acetylene-Ethylene Mixtures. *J. Phys. Chem. B* **2005**, *109*, 12449−12466.
(33) Jones, L. C.; Buras, Z.; Gordon, M. J. Partial Hydrogenation of C_2H_2 on Ag-Doped Pt Nanoparticles. *J. Phys. Chem. C* **2012**, *116*, 12982−12988.
(34) Den Hartog, A. J.; Deng, M.; Jongerius, F.; Ponec, V. Hydrogenation of Acetylene over Various Group Viii Metals - Effect of Particle-Size and Carbonaceous Deposits. *J. Mol. Catal.* **1990**, *60*, 99−108.
(35) Stuck, A.; Wartnaby, C. E.; Yeo, Y. Y.; King, D. A. Microcalorimetric Study of Ethylene on Pt{110}-(1 × 2). *Phys. Rev. Lett.* **1995**, *74*, 578−581.
(36) Yeo, Y. Y.; Stuck, A.; Wartnaby, C. E.; King, D. A. Microcalorimetric Study of Ethylene Adsorption on the Pt{111} Surface. *Chem. Phys. Lett.* **1996**, *259*, 28−36.
(37) Palfi, S.; Lisowski, W.; Smutek, M.; Cerny, S. Calorimetric Studies of Hydrocarbon Adsorption on Metal-Films: V. Hydrocarbons on Platinum. *J. Catal.* **1984**, *88*, 300−312.
(38) Wang, L. X.; Al-Aufi, M.; Pacheco, C. N.; Xie, L. Y.; Rioux, R. M. Polyethylene Glycol (Peg) Addition to Polyethylenimine (Pei)-Impregnated Silica Increases Amine Accessibility During CO_2 Sorption. *ACS Sustainable Chem. Eng.* **2019**, *7*, 14785−14795.
(39) Asplund, S. Coke Formation and Its Effect on Internal Mass Transfer and Selectivity in Pd-Catalysed Acetylene Hydrogenation. *J. Catal.* **1996**, *158*, 267−278.
(40) Huang, X. H.; Xia, Y. J.; Cao, Y. J.; Zheng, X. S.; Pan, H. B.; Zhu, J. F.; Ma, C.; Wang, H. W.; Li, J. J.; You, R.; Wei, S. Q.; Huang, W. X.; Lu, J. L. Enhancing Both Selectivity and Coking-Resistance of a Single-Atom Pd_1/C_3N_4 Catalyst for Acetylene Hydrogenation. *Nano Res.* **2017**, *10*, 1302−1312.
(41) Kelly, T. G.; Chen, J. G. Metal Overlayer on Metal Carbide Substrate: Unique Bimetallic Properties for Catalysis and Electrocatalysis. *Chem. Soc. Rev.* **2012**, *41*, 8021−8034.
(42) Esposito, D. V.; Hunt, S. T.; Kimmel, Y. C.; Chen, J. G. G. A New Class of Electrocatalysts for Hydrogen Production from Water Electrolysis: Metal Monolayers Supported on Low-Cost Transition Metal Carbides. *J. Am. Chem. Soc.* **2012**, *134*, 3025−3033.
(43) Teschner, D.; Borsodi, J.; Wootsch, A.; Revay, Z.; Havecker, M.; Knop-Gericke, A.; Jackson, S. D.; Schlogl, R. The Roles of Subsurface Carbon and Hydrogen in Palladium-Catalyzed Alkyne Hydrogenation. *Science* **2008**, *320*, 86−89.
(44) Ono, S.; Kikegawa, T.; Ohishi, Y. A High-Pressure and High-Temperature Synthesis of Platinum Carbide. *Solid State Commun.* **2005**, *133*, 55−59.
(45) Kuttiyiel, K. A.; Choi, Y.; Hwang, S. M.; Park, G. G.; Yang, T. H.; Su, D.; Sasaki, K.; Liu, P.; Adzic, R. R. Enhancement of the Oxygen Reduction on Nitride Stabilized Pt-M (M = Fe, Co, and Ni) Core-Shell Nanoparticle Electrocatalysts. *Nano Energy* **2015**, *13*, 442−449.
(46) Kuttiyiel, K. A.; Sasaki, K.; Choi, Y. M.; Su, D.; Liu, P.; Adzic, R. R. Nitride Stabilized Ptni Core-Shell Nanocatalyst for High Oxygen Reduction Activity. *Nano Lett.* **2012**, *12*, 6266−6271.
(47) Zhang, Q. W.; Li, J.; Liu, X. X.; Zhu, Q. M. Synergetic Effect of Pd and Ag Dispersed on Al2o3 in the Selective Hydrogenation of Acetylene. *Appl. Catal., A* **2000**, *197*, 221−228.
(48) Pei, G. X.; Liu, X. Y.; Wang, A. Q.; Lee, A. F.; Isaacs, M. A.; Li, L.; Pan, X. L.; Yang, X. F.; Wang, X. D.; Tai, Z. J.; Wilson, K.; Zhang, T. Ag Alloyed Pd Single-Atom Catalysts for Efficient Selective Hydrogenation of Acetylene to Ethylene in Excess Ethylene. *ACS Catal.* **2015**, *5*, 3717−3725.
(49) Hendon, C. H.; Hunt, S. T.; Milina, M.; Butler, K. T.; Walsh, A.; Roman-Leshkov, Y. Realistic Surface Descriptions of Heterometallic Interfaces: The Case of Tiwc Coated in Noble Metals. *J. Phys. Chem. Lett.* **2016**, *7*, 4475−4482.
(50) Leviness, S.; Nair, V.; Weiss, A. H.; Schay, Z.; Guczi, L. Acetylene Hydrogenation Selectivity Control on $PdCu/Al_2O_3$ Catalysts. *J. Mol. Catal.* **1984**, *25*, 131−140.
(51) Sarkany, A.; Weiss, A. H.; Guczi, L. Structure Sensitivity of Acetylene Ethylene Hydrogenation over Pd Catalysts. *J. Catal.* **1986**, *98*, 550−553.
(52) Mears, D. E. Diagnostic Criteria for Heat Transport Limitations in Fixed Bed Reactors. *J. Catal.* **1971**, *20*, 127−131.
(53) Weisz, P. B.; Prater, C. D. Interpretation of Measurements in Experimental Catalysis. *Adv. Catal.* **1954**, *6*, 143−196.
(54) Kresse, G.; Furthmuller, J. Efficiency of Ab-Initio Total Energy Calculations for Metals and Semiconductors Using a Plane-Wave Basis Set. *Comput. Mater. Sci.* **1996**, *6*, 15−50.
(55) Kresse, G.; Joubert, D. From Ultrasoft Pseudopotentials to the Projector Augmented-Wave Method. *Phys. Rev. B: Condens. Matter Mater. Phys.* **1999**, *59*, 1758−1775.
(56) Perdew, J. P.; Burke, K.; Ernzerhof, M. Generalized Gradient Approximation Made Simple. *Phys. Rev. Lett.* **1996**, *77*, 3865−3868.

https://dx.doi.org/10.1021/acscatal.9b04070
ACS Catal. 2020, 10, 6763−6770